How to cite: *Angew. Chem. Int. Ed.* **2021**, *60*, 7735–7743
International Edition: doi.org/10.1002/anie.202013359
German Edition: doi.org/10.1002/ange.202013359

Hydrogen Activation

Kinetics of H_2 Adsorption at the Metal–Support Interface of Au/TiO_2 Catalysts Probed by Broad Background IR Absorbance

*Akbar Mahdavi-Shakib, K. B. Sravan Kumar, Todd N. Whittaker, Tianze Xie, Lars C. Grabow, Robert M. Rioux, and Bert D. Chandler**

Abstract: *H_2 adsorption on Au catalysts is weak and reversible, making it difficult to quantitatively study. We demonstrate H_2 adsorption on Au/TiO_2 catalysts results in electron transfer to the support, inducing shifts in the FTIR background. This broad background absorbance (BBA) signal is used to quantify H_2 adsorption; adsorption equilibrium constants are comparable to volumetric adsorption measurements. H_2 adsorption kinetics measured with the BBA show a lower E_{app} value (23 kJ mol^{-1}) for H_2 adsorption than previously reported from proxy H/D exchange (33 kJ mol^{-1}). We also identify a previously unreported H-O-H bending vibration associated with proton adsorption on electronically distinct Ti-OH metal-support interface sites, providing new insight into the nature and dynamics of H_2 adsorption at the Au/TiO_2 interface.*

Introduction

The unique chemistry at the metal-support interface (MSI) of supported nanoparticle (NP) catalysts has attracted significant research interest in the past decade.[1] Small molecule adsorption at the MSI and the transfer of atoms, protons, and electrons between the metal and support components are fundamentally important processes in catalysis. They impact numerous industrially important reactions including CO/CO_2 hydrogenation to methanol,[2] hydrodeoxygenation,[3] CO oxidation and preferential oxidation,[4] CO_2 electroreduction,[5] and the water-gas shift reaction.[6]

The MSI combines metal functionality with support acid/base chemistry directly at the interface where adsorbates can simultaneously interact with both components. This cooperative bifunctional catalysis is distinct from the well-known traditional bifunctional catalysis, where reactions take place on essentially independent active sites.[7] For example, metal-based chemistries are promoted by support Lewis acid sites in CO_2 hydrogenation over Cu catalysts,[2a] Brønsted acid sites in O_2 activation,[4b,8] and Brønsted base sites in H_2 activation.[6b,9]

Charge transfer between metal and support can also influence catalyst activity and selectivity;[10] in many cases, this is mediated by H atom transfer or spillover.[11] In a particularly compelling example, van Bokhoven and co-workers recently showed activated hydrogen transmission across a reducible oxide support, demonstrating reduction reactions can occur nanometers away from H_2 activation centers.[12] Crossley and co-workers also showed this effect when metallic NPs and the oxide are spatially separated and connected via carbon nanotubes.[13] Similar conclusions have been drawn in examining the role of Pt promoters for Co Fischer–Tropsch catalysts.[14]

While the term "hydrogen spillover" as originally coined by Vannice and Boudart[15] was originally applied to metals that strongly adsorb H_2, the transfer of a proton and electron from metal to support is functionally similar.[16] Yates and co-workers reported broad changes in FTIR difference spectra associated with H_2 adsorption on Au/TiO_2 catalysts, attributing the signal to H spillover, specifically arising from electrons trapped in conduction band edge (CBE) states.[4e,17] A change in the IR light absorbance is expected upon addition of excess electrons to metals and semiconductors,[18] and similar spectral changes have been observed on various types of samples such as single crystals[19] and powders[20] in both UHV and aqueous systems.[21]

The observed spectral changes, which we term the "broad background absorbance" (BBA), can arise when the catalyst interacts with electron donating adsorbates (e.g. CO,[22] H,[20a,b] or H_2)[20c,d,23] or undergoes photo-[20d,24] or electrochemical excitation.[21b,25] The spectral origin of the BBA signal has been attributed to several physio-chemical changes, including (i) intra-band transition of conduction band electrons, (ii) movement of shallow trap electrons into the conduction band,[20a,d] and (iii) surface roughening of the material, leading to an increase in sample scattering and observed decrease in overall light transmission.[9a,22] These suggestions may be related, as conduction band electrons are

[*] A. Mahdavi-Shakib, K. B. S. Kumar, T. N. Whittaker, B. D. Chandler
Department of Chemistry, Trinity University
San Antonio, TX 78212-7200 (USA)
K. B. S. Kumar, L. C. Grabow
Department of Chemical and Biomolecular Engineering
University of Houston
Houston, TX 77204-4004 (USA)
T. Xie, R. M. Rioux, B. D. Chandler
Department of Chemical Engineering
The Pennsylvania State University
University Park, PA 16802 (USA)
E-mail: Bkc5474@psu.edu
L. C. Grabow
Texas Center for Superconductivity at the University of Houston (TcSUH), University of Houston
Houston, TX 77204 (USA)
R. M. Rioux, B. D. Chandler
Department of Chemistry, The Pennsylvania State University
University Park, PA 16802 (USA)
Supporting information and the ORCID identification number(s) for the author(s) of this article can be found under https://doi.org/10.1002/anie.202013359.

expected to populate anti-bonding Ti-O states, which can lengthen surface Ti–O bonds.[9a]

Below, we utilize the BBA phenomenon to selectively probe H_2 adsorption kinetics at the Au/TiO_2 MSI. Active sites at the MSI sites are notoriously difficult to study because they are a small subset of both metal and support sites, resulting in exceedingly low site densities. However, an improved understanding of MSI active sites would aid in designing next generation multi-functional catalysts. Theoretical calculations provide guidelines,[6b] but require experimental observations to inform catalyst design.[4d,9a,17a] We use the BBA signal to determine H_2 adsorption equilibrium constants and show the determined values are consistent with volumetric adsorption measurements. Kinetics studies indicate the BBA signal differentiates H_2 adsorption and H/D exchange kinetics, showing measurable differences in apparent barriers associated with each process.

Additionally, we report a previously unreported spectral signature associated with the active site for H_2 adsorption on these catalysts. These sites are revealed by the formation of a water-like species (nominally $OH_2^{\delta+}$) upon proton addition to MSI hydroxyls. This water-like species, which becomes rapidly saturated during H_2 adsorption experiments, has a distinct vibrational frequency relative to adsorbed water, suggesting a unique electronic interaction between the metal and support.

Results and Discussion

Two Au/TiO_2 catalysts (1 % and 5 % Au with particle sizes 2.7 ± 0.9 and 2.9 ± 0.8 nm, respectively) were prepared via deposition-precipitation as previously reported.[26] A complete materials and methods section, including preparation and characterization details, representative TEM images, and details on FTIR sample preparation are available in the SI. Figure 1 A shows exposure of a freshly reduced sample of 1 % Au/TiO_2 catalyst to a 40 % D_2/N_2 stream results in an immediate increase in the spectral baseline. We refer to this shift as the broad background absorbance (BBA). As described above, the BBA is attributed to the generation of conduction band electrons in the support, which decrease light transmission through the sample either by absorbing IR radiation[4e,17] or by increasing light scattering by the sample.[22]

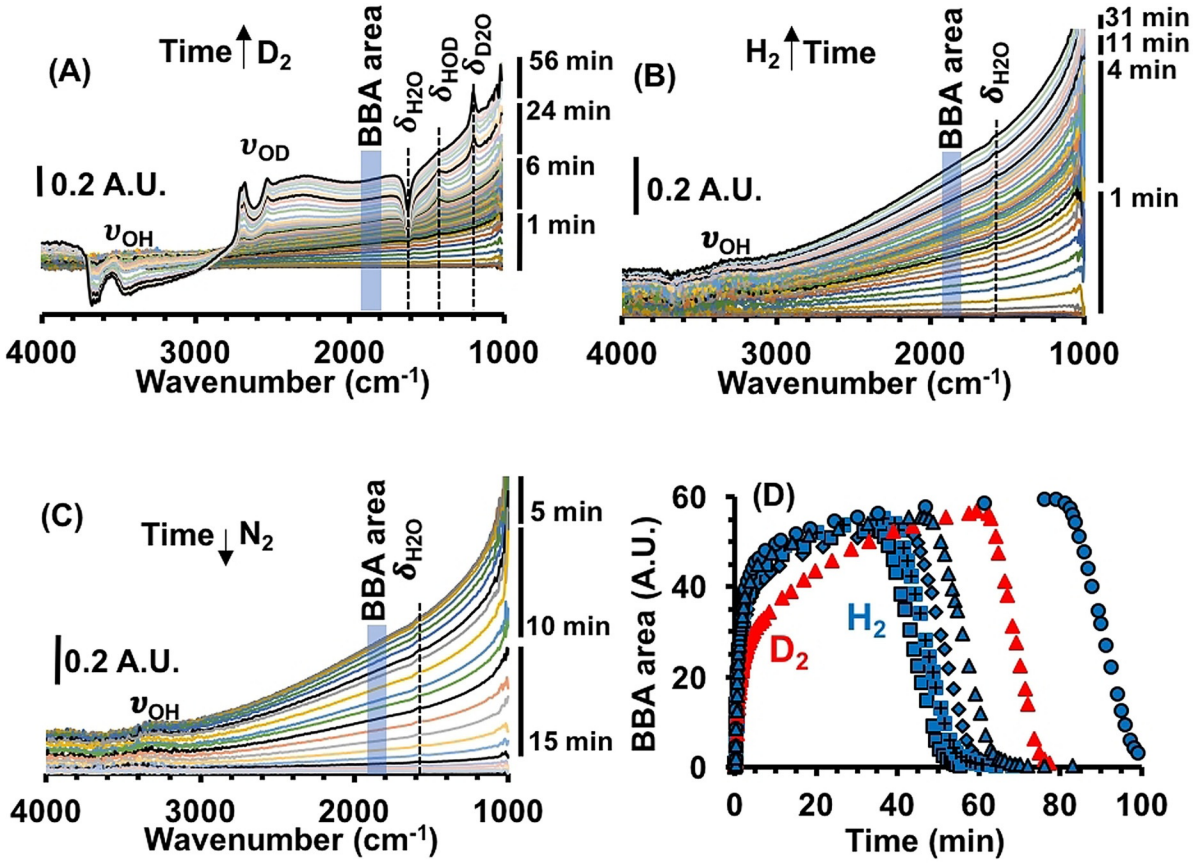

Figure 1. Time evolution of FTIR spectra. A) FTIR spectra recorded after exposing a freshly reduced sample of 1 % Au/TiO_2 to a 40 % D_2/N_2 stream at 71 °C; B) FTIR spectra recorded after exposure of 1 % Au/TiO_2 to a 40 % H_2/N_2 stream at 71 °C. C) FTIR spectra recorded under flowing N_2 after removing H_2 from the feed. Bars on the right side of the panels show time associated with the corresponding spectra. D) BBA profiles recorded during exposure of 1 % Au/TiO_2 to 40 % H_2 at 71 °C. The blue data show the same experiment repeated with varying H_2 exposure times. The red data are collected under 40 % D_2 at 71 °C. All spectra were recorded as difference spectra referenced to the single beam spectrum of the sample immediately before exposure to H_2 or D_2. Reported areas are the entire integrated area under the spectrum from 1800–1900 cm^{-1} referenced to this baseline. The drop in the BBA intensity corresponds to switching the H_2 (D_2) flow off.

The BBA signal increases rapidly for approximately one minute; after this time, broad absorbances at $\approx 2500\ cm^{-1}$ (ν_{OD}), $\approx 1430\ cm^{-1}$ (δ_{HOD}), and $\approx 1200\ cm^{-1}$ (δ_{D_2O}) appear. The negative bands near $3500\ cm^{-1}$ in the difference spectra (Figure 1A), indicate a loss of surface hydroxyl groups. Exposure to D_2 results in a regime of fast BBA evolution followed by a regime where the BBA evolves more slowly and H/D exchange begins (see below). The BBA reached almost 30% of its maximum intensity in this initially fast regime (≈ 1 min); whereas nearly an hour was required for complete H/D exchange (see below).

The BBA signal also arises in experiments where no H/D exchange was possible, that is, H_2 adsorption on a protonated surface (Figure 1B). As above, the BBA signal appears immediately upon exposure to H_2, intensifies quickly over the first few minutes, followed by slower evolution of the BBA intensity. The corresponding experiment examining D_2 adsorption on a pre-deuterated hydroxyl surface has nearly identical BBA features (see SI). The H_2 adsorption experiment (Figure 1B) also shows the appearance of weak bands at $\approx 3300\ cm^{-1}$ and $\approx 1580\ cm^{-1}$. These bands are assignable to ν_{OH} and δ_{H_2O} stretching and bending bands, respectively, and indicate formation of a water-like species (WLS) as H_2 first adsorbs on the catalyst. This is consistent with our previous density functional theory (DFT) and experimental results, which indicate H_2 adsorption occurs via heterolytic dissociation at the MSI.[9a,b] The BBA signal is considerably more intense than the ν_{OH} and δ_{H_2O} bands, indicating the BBA signal offers a sensitive method for monitoring H_2 adsorption in these systems. Figure 1C shows the spectra recorded after H_2 flow was switched to N_2 (i.e., pressure swing desorption). The BBA signal and bands associated with a WLS (see below) gradually decreased in intensity until all features were eliminated (≈ 25 min.). This process is completely reversible, consistent with the well-known weak adsorption of H_2 on Au catalysts.[2d,27]

The BBA signal intensity can be quantified by measuring the total area under the spectrum from 1800 to $1900\ cm^{-1}$, as reported previously.[9a,b,22] This spectral range, shown with a blue bar in Figure 1, was selected due to the relatively large changes in BBA intensity and minimal interference from other features (e.g. hydroxyls, water). We note other frequency ranges yield similar results (see SI for more details). Figure 1D shows plots of the BBA area versus time for several adsorption experiments. The BBA signal evolution is highly reproducible; in five repeat experiments, it showed similar evolution over time and similar total increases in intensity. The BBA intensity always returned to zero when H_2 was removed, confirming the reversibility of the underlying chemistry.

Figure 1D includes a time profile for D_2 adsorption under similar conditions. The BBA values after one hour of adsorption are essentially the same for H_2 and D_2, consistent with the proposed structural/electronic origins of the BBA.[9a,22] The D_2 adsorption profile also indicates somewhat slower D_2 adsorption kinetics. Since H_2 adsorption is dissociative, a kinetic isotope effect is expected, and indeed required if the BBA kinetics report on activated $H_2(D_2)$ adsorption. The small isotope effects are fully consistent with the conclusion the BBA arises from the elementary step of heterolytic H_2 dissociation at the MSI.[9a]

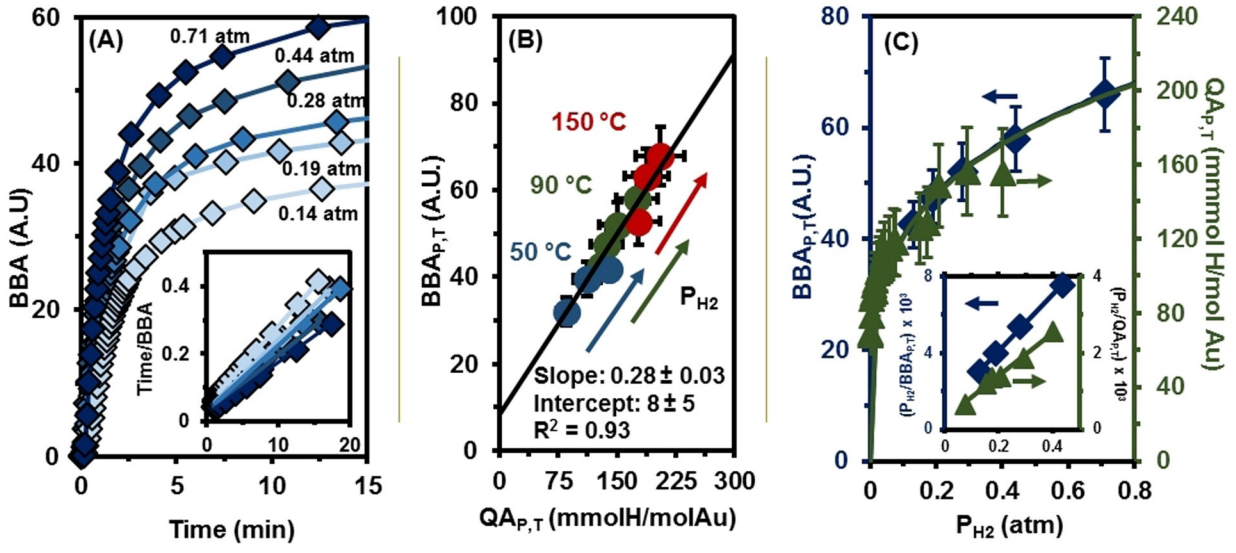

Figure 2. Quantitative H_2 adsorption at 90°C. A) Integrated BBA intensity as a function of time measured at several H_2 pressures. The inset shows the plots used to extract $BBA_{P,T}$ values for each experiment. Inset lines are linear fits to the data (details in the SI). B) $BBA_{P,T}$ values plotted against the quantity of H_2 adsorbed ($QA_{P,T}$) measured in static volumetric adsorption experiments. C) Adsorption isotherms prepared from (i) $BBA_{P,T}$ values of FTIR experiments (blue diamonds) and (ii) H_2 uptake from volumetric chemisorption experiments (green triangles). The line shows the fit of all the experimental data to a Freundlich adsorption isotherm. The inset shows linearized Langmuir plots used to estimate the equilibrium constant for P_{H_2} from 0.1–0.45 atm. Error bars correspond to 15% uncertainty in the volumetric adsorption and 10% uncertainty in the BBA measurements; these uncertainty estimates were based on several repeat experiments.

Quantitative analysis of BBA profiles

Figure 2 A shows the evolution of the BBA signal during H_2 adsorption at 90 °C. The $BBA_{P,T}$ value for each adsorption experiment was determined by treating the BBA profile as a saturation curve and extracting $BBA_{P,T}$ (the full BBA signal at a given temperature and P_{H_2} when the adsorption time approaches infinity) from the slope of the linearized form of the data (inset in Figure 2 A). A complete description of the data treatment and plots are provided in the SI. Figure 2 A also shows the $BBA_{P,T}$ value increases with P_{H_2}, suggesting the BBA signal correlates directly with the amount of adsorbed H_2. To quantify the weak, reversible H_2 adsorption shown in Figure 1, we measured reversible H_2 adsorption isotherms in a standard volumetric adsorption instrument. Figure 2 B shows a strong linear correlation between the $BBA_{P,T}$ values and the quantity of adsorbed H_2 (QA). This allows us calibrate and quantify the BBA signal in terms of the quantity of adsorbed H_2 (details in the SI).

The P_{H2} dependence of the $BBA_{P,T}$ and $QA_{P,T}$ values is shown in Figure 2 C; the added line fits of all the experimental data to a Freundlich adsorption isotherm. This suggests the enthalpy of adsorption varies over wide ranges of H_2 coverage. CO adsorption on Au and Pd-Au catalysts shows coverage-dependent adsorption constants;[28] the volumetric and BBA data suggests H_2 adsorption is similarly coverage dependent. However, changes to the adsorption constant (K_{H_2}) are expected to be small when the H_2 coverage is relatively constant, making the Langmuir description a reasonable approximation when QA values are similar. The inset in Figure 2 C shows both the BBA and QA data sets are well-described by linear Langmuir isotherms for H_2 pressures from 0.1 to 0.45 atm H_2 (QA ≈ 150 mmol H mol^{-1} Au). The goodness of these fits justifies the Langmuir approximation and allows us to estimate K_{H_2} for this pressure range.

Table 1: FTIR and volumetric adsorption data determined at 90 °C and $P_{H_2} = 0.1$–0.45 atm.

		Catalyst	
		1 % Au	4.5 % Au
	Au d_{avg} [nm]	2.7 ± 0.9	2.9 ± 0.8
	% perimeter sites	3.5	3.3
K_{H_2} [atm^{-1}]	BBA data	12 ± 2	13 ± 2
	Vol. ads data	20 ± 6	21 ± 4
$-\Delta G_{ads}$ [kJ mol^{-1}]	BBA data	7 ± 1	8 ± 1
	Vol. ads data	9 ± 3	9 ± 4
$-\Delta H_{ads}$ [kJ mol^{-1}]	BBA data	40 ± 3	41 ± 3
	Vol. ads data	41 ± 3	41 ± 4
QA_{H_2} ($P_{H_2} = 0.5$ atm)	mol H/mol Au	0.18 ± 0.01[a]	0.10 ± 0.01[a]
BBA calibration	mmol H/mol Au/ BBA area[b]	3.0 ± 0.8	1.4 ± 0.4

[a] Values correspond to 5.1 ± 0.8 and 3.0 ± 0.3 $H/Au_{perimeter}$ for the 1 % and 4.5 % catalysts, respectively. [b] For BBA changes from 1800–1900 cm^{-1}.

Extracted K_{H_2} values can be interpreted as ΔH_{ads} values by assuming a constant ΔS_{ads} of −90 J mol^{-1} K. While studying propane hydrogenolysis over Ru/Al_2O_3, Tsjeng and Anderson determined a ΔS_{ads} for H_2 of −87.0 J mol^{-1} K at 411 K.[29] As discussed by Vannice and co-workers, this value likely represents an upper bound for the true value of the entropy associated with dissociative adsorption of H_2 on a metal.[30] Campbell and Sellers' method for estimating ΔS_{ads} yields nearly the same value (−91.5 J mol^{-1} K).[31] This analysis yields $-\Delta H_{ads}$ values of about −40 kJ mol^{-1} for both experiments and both catalysts. This is ≈ 20 kJ mol^{-1} weaker than reported for CO adsorption on Au,[28] and seems reasonable given the well-known weak binding of H_2 to Au.[2d,27]

Several groups have provided a theoretical basis for estimating the number of added electrons associated with a BBA signal, using other model systems. Bürgi et al. used the Drude model to describe BBA changes in attenuated total reflection (ATR) spectra of a Pd thin film.[32] Their work showed a linear relationship between the number of added electrons and expected BBA intensity. Wöll et al. interpreted changes to the BBA intensity in transmission FTIR spectra with the Drude-Zener model to estimate the number of electrons added to ZnO.[20b] Consistent with these theoretical models, we observe a linear relationships between H_2 pressure and (i) the BBA signal (Figure 2 B and Figure S10) and (ii) volumetric H_2 adsorption. Accordingly, the BBA intensity may be useful for tracking electron addition to the catalyst. While a further exploration of the details of these interactions is beyond the scope of this paper, these models provide a solid fundamental foundation for using the BBA signal as a measure of H_2 adsorption on these catalysts.

This allows us to calibrate the BBA signal to the amount of H_2 adsorbed on the catalyst (details in the SI). For Au/TiO_2, the low H_2 uptake and weak nature of the interaction between H_2 and the catalyst have impeded quantitative evaluation of this interaction for more than 20 years. The BBA signal is significantly more sensitive than individual vibrational bands (e.g. ν_{OH}) or volumetric chemisorption, enabling a new examination of H_2 adsorption on these and related catalysts. Additionally, IR experiments can distinguish H_2 adsorption from other surface processes (e.g. H/D exchange), and have time resolution that is sufficiently sensitive to evaluate adsorption kinetics. This provides significant new insight into H_2 adsorption and H/D exchange kinetics, as we show below. These are substantial advantages to the BBA methodology that afford measurements currently unavailable via volumetric adsorption techniques alone.

Kinetic Analysis using BBA

The initial time data in Figure 2 contain kinetic information appropriate for initial rate analysis; rate data and plots are available in the SI. The kinetics are well behaved, yielding a reaction order for H_2 adsorption of 0.6 (Table 2). The measured H_2 reaction order during H_2 oxidation catalysis is essentially the same.[9a,b] While these two values measure slightly different quantities (H_2 adsorption versus H_2 oxidation, which includes both adsorption and reaction with O_2), H_2

Table 2: Kinetic parameters of H_2 and D_2 adsorption on Au/TiO_2.

	H_2 rxn order	E_{app} [kJ mol^{-1}]	reference
BBA H_2 ads	0.6 ± 0.1[b]	23 ± 2[e]	This work
H_2 Ox. kinetics	0.64 ± 0.05[c]	31 ± 3[f]	[9a]
H/D exchange[a]	0.6 ± 0.06[d]	33 ± 2[g]	This work
H_2-D_2 equilibration	1	36 ± 1[h]	[33]

[a] Measured by monitoring the loss of δ_{H_2O} after exposure to D_2. [b] P_{H_2}: 0.19–0.86 atm, temperature: 90 °C. [c] P_{H_2}: 0.03–0.6 atm, temperature: 60 °C. [d] P_{H_2}: 0.14–0.81 atm, temperature: 71 °C. [e] temperature: 21–51 °C, P_{H_2}: 0.4 atm. [f] P_{H_2} temperature: 45–60 °C, P_{H_2}: 0.8 atm. [g] temperature: 51–71 °C, P_{D_2}: 0.4 atm. [h] temperature: 80–180 °C, 6 torr of H_2 and 6 torr of D_2.

oxidation kinetics depend strongly on H_2 adsorption, so reasonable agreement between the H_2 dependencies is expected. Table 2 also shows the results of a BBA Arrhenius study conducted with $P_{H_2} = 0.44$ atm (data in the SI). Results from this study are discussed in the section on H/D exchange below.

Figure 1 D shows the BBA decay process when H_2 (or D_2) is removed from the feed is also highly reproducible. The linear portion of the decay plots (available in the SI) yield an average H_2 evolution rate of 3.9 ± 0.1 BBA min^{-1}. Based on comparisons with volumetric H_2 adsorption data (see below), this corresponds to 0.3 ± 0.1 μmol H_2/g_{cat} min^{-1}. These data suggest the BBA can potentially be used to study structure–reactivity relationships in photochemical H_2 evolution or to study the dynamics of photogenerated charge carriers and electron-hole recombination rates.[24,34] While such a study is outside the scope of this paper, it highlights the potential value of further investigation and application of BBA studies.

Deconvolution of H/D Exchange Kinetics from H_2 and D_2 Adsorption Kinetics

Since H_2 adsorption kinetics are difficult to measure, H_2-D_2 equilibration and/or exchange reactions are commonly used as a proxy for H_2 activation kinetics.[9a,33,35] These reactions are widely understood to be dominated by H_2 activation, and are therefore appropriate in the absence of more direct methods. Indeed, both our initial evaluation of H_2 oxidation[9a,b] and Fujitani's H_2-D_2 equilibration study[33] attributed E_{app} values of 30–35 kJ mol^{-1} to the barrier for H_2 adsorption. However, H/D exchange processes are more complex than H_2 adsorption, involving proton transport, recombination, and desorption. A distinguishing feature of the BBA technique is that it has the potential to differentiate H_2 adsorption from H/D exchange.

The experiment presented in Figure 1 A can be used to examine H/D exchange kinetics by monitoring the δ_{H_2O} band disappearance and/or the appearance of the δ_{D_2O} band. Time profiles for these IR bands (Figure 3) show the rapid evolution of the BBA signal followed by more gradual changes in water isotope speciation (H_2O, HOD, D_2O). For the D_2 adsorption experiment shown in Figure 1 A, loss of the δ_{H_2O} band was followed to monitor H/D exchange kinetics. This allows differentiation between H_2 adsorption kinetics

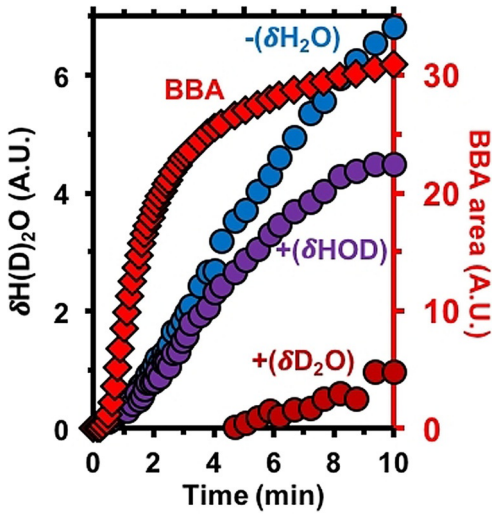

Figure 3. Evolution of IR band intensities (BBA, HOD, and D_2O growth; H_2O loss) during D_2 adsorption (40% D_2/N_2 at 71 °C) on 1% Au/TiO_2. The integrated areas were extracted from the spectra shown in Figure 1 A.

(via the BBA signal) and H/D exchange rates (via production or loss of D_2O and H_2O, respectively). Table 2 shows H_2 adsorption, H/D exchange, and H_2 oxidation all have essentially the same P_{H2} dependence, consistent with the notion that all three processes are primarily controlled by $H_2(D_2)$ adsorption.

The evolution of each of these bands can be monitored during Arrhenius studies (details in the SI). This allows for the simultaneous determination of the H_2 adsorption and H/D exchange apparent barriers from a single data set, simply by evaluating different signals during a single experiment. The determined apparent barrier for H/D exchange (33 kJ mol^{-1}) is essentially the same as the apparent activation energy reported by Fujitani et al. for H_2-D_2 equilibration over a series of Au catalysts (36 kJ mol^{-1}).[33] However, the IR experiments show the apparent barrier for H/D exchange is considerably higher ($\approx 50\%$) than the H_2 adsorption barrier measured in the same set of experiments. The statistically significant differences in E_{app} values indicates they are associated with two distinct processes: 20–25 kJ mol^{-1} for H_2 adsorption and 30–35 kJ mol^{-1} for H/D exchange. This suggests surface transport and/or recombination processes[36] play a larger role in in H_2-D_2 equilibration and H_2 oxidation kinetics than previously considered.

Identification of H_2 Activation Sites at the Metal-Support Interface.

In examining the H/D exchange kinetics, we noticed a consistent delay between the initial evolution of the BBA signal and the onset of H/D exchange. To better illustrate this relationship, Figure 4 shows changes to the δ_{H_2O} band plotted vs. BBA intensity during D_2 adsorption for several D_2 pressures. Regardless of P_{D_2}, the BBA and δ_{H_2O} signals follow essentially the same trajectory (Figure 4 B). This is also

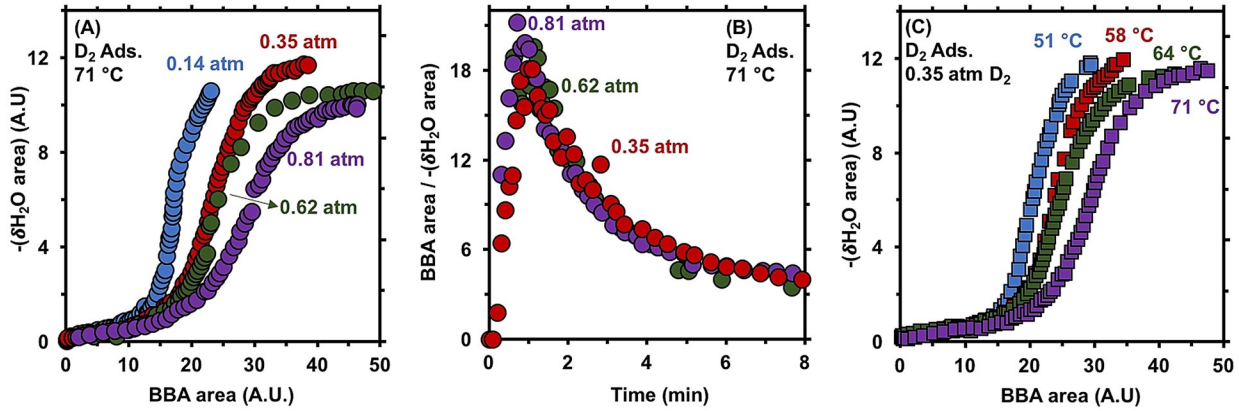

Figure 4. Induction time in H/D exchange of surface water molecules after exposure to D_2. A) loss of water bending band intensity versus integrated BBA area at 71 °C for four different D_2 pressures; B) ratio of integrated BBA to water bending band intensity as a function of time; C) loss of water bending band intensity versus integrated BBA area at 0.35 atm D_2 at four different temperatures.

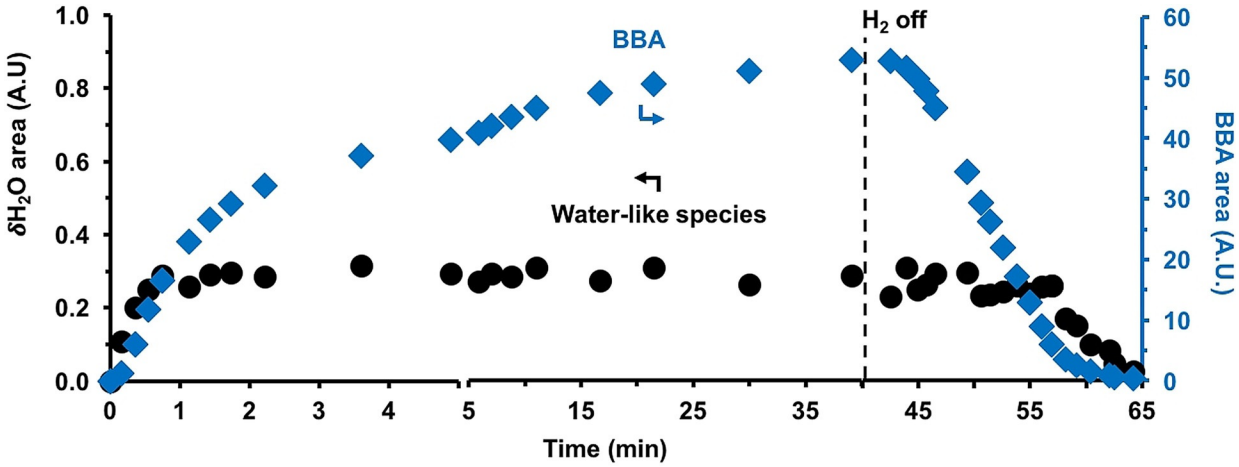

Figure 5. Time evolution of the integrated areas of WLS bending band and BBA signal after exposing the 1% Au/TiO_2 catalyst to 40% flowing H_2/N_2 at 71 °C. The integrated areas were extracted from the spectra shown in Figure 1 B&C.

observed in plots of the BBA/δ_{H_2O} band ratio versus time (see SI) and in Arrhenius studies (Figure 4C). These adsorption experiments have widely different reaction rates, yet the relationship between the BBA and δ_{H_2O} areas is essentially constant. This suggests a critical concentration of protons/electrons on the surface must accumulate before H/D exchange can begin.

Closer examination of the H_2 adsorption spectra in Figure 1 shows the appearance of a very weak signal around $\approx 1600\ cm^{-1}$. Figure 5 examines the evolution of this spectral band and the BBA signal. Both the δ_{H_2O} band intensity and BBA signals increased linearly over the first minute after exposure to H_2, but then diverge, with the BBA feature evolving as described above. The δ_{H_2O} band plateaued after ≈ 1 min, then remained remarkably consistent throughout the remainder of the experiment. Upon removing H_2, the BBA band begins to disappear while the δ_{H_2O} band does not change until the BBA intensity approaches zero. This behavior is inconsistent with adsorbed water, so we attribute this bending band a "water-like species" (WLS).

The value of ≈ 15 BBA absorbance units for WLS saturation in the H_2 adsorption experiments is essentially the same as the value required for the onset of H/D exchange. This suggests the WLS plays a fundamental role in H_2 (and D_2) adsorption. Using the calibration from volumetric chemisorption, the BBA intensity of ≈ 15 area units corresponds to $\approx 0.04 \pm 0.01$ H/Au_{tot}, or approximately 1 WLS per Au_{per} site (per = perimeter; details in the SI). This value strongly suggests the WLS is associated with protons adsorbed on Ti-OH groups at the MSI.

We examined a 4.5% Au/TiO_2 catalyst with similar Au particle size (2.9 ± 0.8 nm) to further confirm the role of WLS in H_2 adsorption. Figure 6 shows the higher Au loading resulted in faster adsorption kinetics and more intense δ_{H_2O} and ν_{OH} bands. The 4.5% Au catalyst showed the same adsorption profile over time, but the WLS δ_{H_2O} vibration is clearly discernable at $\approx 1580\ cm^{-1}$. This is a considerably lower frequency than is attributable to water adsorbed on TiO_2, which is typically found around ≈ 1640–$1620\ cm^{-1}$.[37] Extracted ν_{OH} areas for the data in Figure 6 (see SI) follow essentially the same trend as δ_{H_2O} band, rising rapidly and plateauing after ≈ 1 min. These bands are therefore also attributable to the WLS.

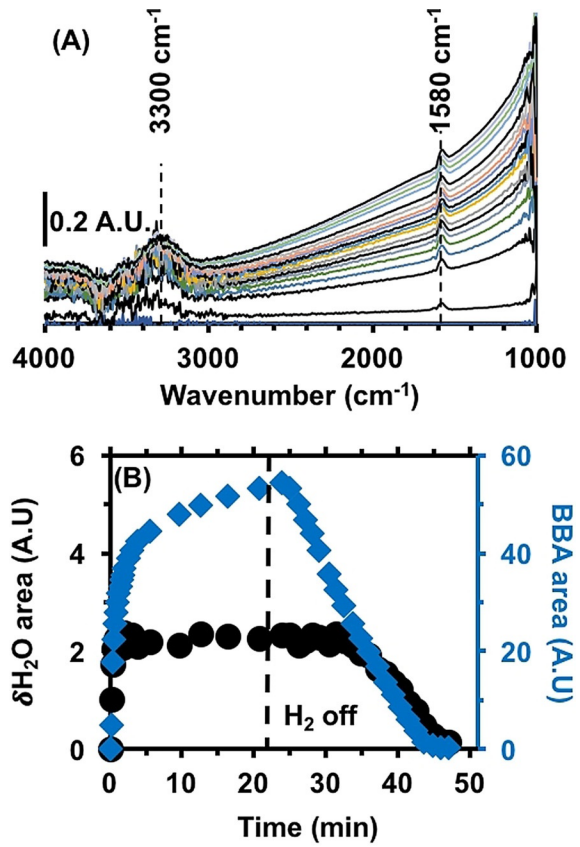

Figure 6. H_2 adsorption on 4.5% Au/TiO_2. A) difference FTIR spectra recorded after exposure to 40% flowing H_2/N_2 at 71 °C. B) Integrated δ_{H_2O} (of WLS) and BBA areas versus time.

Based on all the above data, 1580 cm^{-1} band associated with the WLS is attributed to proton transfer to support hydroxyl groups at the MSI. The resulting protonated Ti-OH group appears to be a very strongly adsorbed $OH_2^{\delta+}$ species. The spectral overlap between the active hydroxyls and all the other hydroxyls on the support make them indistinguishable from one another with FTIR spectroscopy; the active hydroxyls are only observable as the WLS present after H_2 adsorption. Previous studies showed the addition of atomic hydrogen to a bare TiO_2 support does not produce a similar WLS.[20a] Thus, the unique bending vibration attributable to the WLS suggests it arises from an electronically unique Ti-OH group.

Figure 6B shows the WLS species saturates at ≈22 BBA units on the 4.5% Au/TiO_2 catalyst. Employing the same calibration protocol using volumetric chemisorption experiments (see SI), the 22 BBA unit value corresponds to 0.031 ± 0.009 H/Au_{tot} or 0.9 ± 0.3 WLS per Au_{per} site. Given all the measurements involved (chemisorption, BBA_{max} determination, analysis of TEM data, IR peak areas), this is good agreement between the two catalysts. These values assume every adsorbed H_2 molecule is rapidly converted to 2 protons at the MSI; the associated electrons are transferred to the TiO_2 conduction band, where they are observed as the BBA. These are reasonable assumptions given our previous experimental and computational evidence involving H_2 adsorption on Au catalysts. This evidence includes: (i) H_2 adsorption occurs through a heterolytic H_2 activation mechanism at the Au/TiO_2 interface, (ii) H_2 adsorption involves electron transfer to the support, and (iii) Au-H deprotonation by the support is thermodynamically favored with a lower barrier than H_2 adsorption.[9a,b]

Thus, it appears most of the Au perimeter sites are sufficiently close to reactive surface hydroxyls to enable H_2 activation. Coupled to the unique bending vibration attributable to the WLS (1580 cm^{-1}) these results indicate the active hydroxyl groups are somehow modified by their close electronic interactions with the Au nanoparticles. In other words, the combination of electronically distinct Ti-OH groups and Au atoms at the MSI appear to be the active site for H_2 adsorption and desorption on these catalysts. Fujitani et al. recently reported TPD experiments using Au nanoparticles supported on single-crystal TiO_2 (110) model systems, finding the amount of dissociated water tracked with number of Au perimeter sites, and that CO oxidation activity correlated with the number of these interface sites.[4c]

H_2 Adsorption after Saturation of the Metal-Support Interface

The BBA signal increases 2–3 fold after the WLS signal saturates, indicating H_2 adsorption and electron transfer to the support continues long after the active sites are saturated with protons. While it is surprising the maximum observable concentration of WLS is reached so quickly, it helps explain the volumetric chemisorption data, which show total H_2 uptakes are several multiples of the number of Au perimeter sites (Table 1). We find no evidence in the IR spectra for the formation of Au-H species on the nanoparticle surface (2100–2200 cm^{-1}).[38] While such a species would likely be difficult to observe, DFT calculations indicate Au-H is thermodynamically unstable relative to deprotonation by Ti-OH.[9a,b] This suggests H_2 adsorption beyond WLS formation results in protons and electrons transferred to the support rather than stored in/on the Au. While the electrons are observable via the BBA signal, we are unable to immediately discern the fate of the accompanying protons.

The additional adsorbed H_2 appears to reside in a form that promotes surface proton transfer,[36] as evidenced by the onset of H/D exchange with support hydroxyls once the WLS δ_{H_2O} band saturates. We considered the possibility that new hydroxyl groups are formed; however, O-H stretching frequencies associated with the WLS are observed immediately upon adsorption. This band stops evolving with the δ_{H_2O} band (see SI), providing no evidence for the generation of additional surface hydroxyls beyond those associated with the WLS.

In single crystal UHV experiments, several groups found added protons become invisible to surface sensitive methods such as HREELS and STM at high temperatures. In some cases, this observation has been attributed to proton diffusion into the TiO_2 bulk.[39] DFT calculations showed H^+ adsorption onto surface -OH groups is far more stable than sub-surface sites (see SI). Further, rapid H/D exchange between adsorbed H/D and surface hydroxyls begins when the WLS signal saturates, indicating that the "missing" protons are readily available to the surface. Thus, while proton migration into the

bulk is not completely unthinkable for these catalysts, we believe it is unlikely in these experiments.

A more plausible explanation is that the additional protons are stored on the support as surface hydronium ions.[40] We distinguish between hydronium, which arises from proton transfer to strongly adsorbed water, and the WLS, which arises from proton transfer to a Ti-OH group at the MSI. Hydronium ions on solid surfaces have a vibrational band around 1100–1200 cm^{-1}.[41] This band is relatively weak and is likely masked by lattice vibrations, making it difficult to observe on an oxide material. Hydronium should exchange with surface hydroxyls, so the onset of rapid H/D exchange with the onset of surface hydronium production supports this conclusion. Increased H/D exchange rates were reported upon generation of hydronium on FeO;[40c] our results are consistent with that finding. Thus, the presence of surface hydronium ions, which are difficult to observe, makes good chemical sense and provides a very reasonable explanation for both the rapid H-D exchange and the unobserved protons.[42]

Conclusion

Although H_2 is IR inactive, H_2 adsorption on Au/TiO_2 catalysts transfers electron density into the support, generating a broad shift in the spectral baseline. This broad background absorbance (BBA) is readily integrated and quantified, providing a new tool for examining H_2 adsorption on Au/TiO_2 catalysts and similar materials. Thermodynamic quantities determined with the BBA are consistent with values determined from volumetric adsorption; further, the significantly higher sensitivity of the BBA allows for monitoring H_2 adsorption kinetics.

The BBA methods allowed us to directly measure H_2 adsorption kinetics as a function of temperature and pressure. Further, by monitoring the BBA signal and H_2O or D_2O bands, a single experiment can differentiate H_2 adsorption and H/D exchange kinetics. The extracted activation barrier for H_2 adsorption is significantly lower than previously reported values determined with proxy reactions such as H_2-D_2 equilibration and H_2 oxidation.

Close examination of H_2 adsorption spectra allowed us to identify a clear spectroscopic signature associated with electronically unique hydroxyl groups at the metal-support interface. Proton transfer to these MSI hydroxyls results in a water-like species with bending vibration at approximately 1580 cm^{-1}; this is significantly shifted from vibrations associated with adsorbed water or other hydroxyls. Correlations with volumetric chemisorption data suggest most of the Au perimeter sites are sufficiently close to an active Ti-OH to serve as a H_2 activation site. This work represents the clearest spectroscopic evidence to date of H_2 adsorption and activation directly at the metal-support interface.

Acknowledgements

The authors gratefully acknowledge the National Science Foundation (Awards CBET-1803769 and CHE-1566301) and the Research Corporation for Science Advancement for supporting this work. K.B.S.K. and L.C.G. acknowledge financial support from NSF CBET-1454384. T.Z. and RMR acknowledge the financial support from NSF CBET-1803808. The authors thank Lauren Rich for her assistance in collecting IR spectra. Computational resources were provided by the uHPC cluster managed by the University of Houston and acquired through NSF-MRI award number 1531814. This work used the Extreme Science and Engineering Discovery Environment (XSEDE), which was supported by NSF grant number ACI-1053575.[43] We also acknowledge the use of computational resources provided by the National Energy Research Scientific Computing Center, a DOE Office of Science User Facility supported by the Office of Science of the US Department of Energy under contract number DE-AC02-05CH11231. We also acknowledge the use of the Opuntia/Sabine/Carya Clusters and the advanced support from the Research Computing Data Core at the University of Houston.

Conflict of interest

The authors declare no conflict of interest.

Keywords: gold catalyst · hydrogen activation · infrared spectroscopy · metal–support interface · hydroxyl groups

[1] T. W. van Deelen, C. Hernández Mejía, K. P. de Jong, *Nat. Catal.* **2019**, *2*, 955 – 970.

[2] a) E. Lam, K. Larmier, G. Noh, P. Wolf, A. Comas-Vives, C. Coperet, J. J. Corral-Perez, A. Urakawa, A. Comas-Vives, A. Urakawa, *Angew. Chem. Int. Ed.* **2019**, *58*, 13989 – 13996; *Angew. Chem.* **2019**, *131*, 14127 – 14134; b) S. Kattel, P. Liu, J. G. Chen, *J. Am. Chem. Soc.* **2017**, *139*, 9739 – 9754; c) N. Rui, F. Zhang, K. Sun, Z. Liu, W. Xu, E. Stavitski, S. D. Senanayake, J. A. Rodriguez, C.-J. Liu, *ACS Catal.* **2020**, *10*, 11307; d) M. Sankar, Q. He, R. V. Engel, M. A. Sainna, A. J. Logsdail, A. Roldan, D. J. Willock, N. Agarwal, C. J. Kiely, G. J. Hutchings, *Chem. Rev.* **2020**, *120*, 3890 – 3938.

[3] R. C. Nelson, B. Baek, P. Ruiz, B. Goundie, A. Brooks, M. C. Wheeler, B. G. Frederick, L. C. Grabow, R. N. Austin, *ACS Catal.* **2015**, *5*, 6509 – 6523.

[4] a) J. Saavedra, T. Whittaker, Z. Chen, C. J. Pursell, R. M. Rioux, B. D. Chandler, *Nat. Chem.* **2016**, *8*, 584 – 589; b) J. Saavedra, H. A. Doan, C. J. Pursell, L. C. Grabow, B. D. Chandler, *Science* **2014**, *345*, 1599 – 1602; c) T. Fujitani, I. Nakamura, A. Takahashi, *ACS Catal.* **2020**, *10*, 2517 – 2521; d) I. X. Green, W. Tang, M. Neurock, J. T. Yates, Jr., *Science* **2011**, *333*, 736 – 739; e) I. X. Green, W. Tang, M. Neurock, J. T. Yates, Jr., *Angew. Chem. Int. Ed.* **2011**, *50*, 10186 – 10189; *Angew. Chem.* **2011**, *123*, 10368 – 10371.

[5] D. Gao, Y. Zhang, Z. Zhou, F. Cai, X. Zhao, W. Huang, Y. Li, J. Zhu, P. Liu, F. Yang, G. Wang, X. Bao, *J. Am. Chem. Soc.* **2017**, *139*, 5652 – 5655.

[6] a) M. M. Kauppinen, M. M. Melander, A. S. Bazhenov, K. Honkala, *ACS Catal.* **2018**, *8*, 11633 – 11647; b) N. C. Nelson, J. Szanyi, *ACS Catal.* **2020**, *10*, 5663 – 5671; c) Y. Zhang, J. Zhang, B. Zhang, R. Si, B. Han, F. Hong, Y. Niu, L. Sun, L. Li, B. Qiao, K. Sun, J. Huang, M. Haruta, *Nat. Commun.* **2020**, *11*, 558.

[7] G. Kumar, E. Nikolla, S. Linic, J. W. Medlin, M. J. Janik, *ACS Catal.* **2018**, *8*, 3202 – 3208.

[8] J. Saavedra, C. J. Pursell, B. D. Chandler, *J. Am. Chem. Soc.* **2018**, *140*, 3712 – 3723.

[9] a) K. B. Sravan Kumar, T. N. Whittaker, C. Peterson, L. C. Grabow, B. D. Chandler, *J. Am. Chem. Soc.* **2020**, *142*, 5760 – 5772; b) T. Whittaker, K. B. S. Kumar, C. Peterson, M. N. Pollock, L. C. Grabow, B. D. Chandler, *J. Am. Chem. Soc.* **2018**, *140*, 16469 – 16487; c) J. L. Fiorio, R. V. Gonçalves, E. Teixeira-Neto, M. A. Ortuño, N. López, L. M. Rossi, *ACS Catal.* **2018**, *8*, 3516 – 3524.

[10] a) X. Li, J. Lin, L. Li, H. Yike, X. Pan, S. E. Collins, Y. Ren, Y. Su, L. Kang, X. Liu, Y. Zhou, H. Wang, A. Wang, B. Qiao, X. Wang, T. Zhang, *Angew. Chem. Int. Ed.* **2020**, *59*, 19983 – 19989; *Angew. Chem.* **2020**, *132*, 20158 – 20164; b) J. Zhang, S. Deo, M. J. Janik, J. W. Medlin, *J. Am. Chem. Soc.* **2020**, *142*, 5184 – 5193.

[11] C. R. O'Connor, M. A. van Spronsen, T. Egle, F. Xu, H. R. Kersell, J. Oliver-Meseguer, M. Karatok, M. Salmeron, R. J. Madix, C. M. Friend, *Nat. Commun.* **2020**, *11*, 1844.

[12] W. Karim, C. Spreafico, A. Kleibert, J. Gobrecht, J. VandeVondele, Y. Ekinci, J. A. van Bokhoven, *Nature* **2017**, *541*, 68 – 71.

[13] N. M. Briggs, L. Barrett, E. C. Wegener, L. V. Herrera, L. A. Gomez, J. T. Miller, S. P. Crossley, *Nat. Commun.* **2018**, *9*, 3827.

[14] S. K. Beaumont, S. Alayoglu, C. Specht, W. D. Michalak, V. V. Pushkarev, J. Guo, N. Kruse, G. A. Somorjai, *J. Am. Chem. Soc.* **2014**, *136*, 9898 – 9901.

[15] M. Boudart, M. A. Vannice, J. E. Benson, *Z. Phys. Chem. Neue Folge* **1969**, *64*, 171.

[16] R. Prins, *Chem. Rev.* **2012**, *112*, 2714 – 2738.

[17] a) I. X. Green, W. Tang, M. Neurock, J. T. Yates, Jr., *Acc. Chem. Res.* **2014**, *47*, 805 – 815; b) D. A. Panayotov, J. T. Yates, *Chem. Phys. Lett.* **2005**, *410*, 11 – 17.

[18] A. F. Gibson, *J. Sci. Instrum.* **1958**, *35*, 273 – 278.

[19] H. Sezen, M. Buchholz, A. Nefedov, C. Natzeck, S. Heissler, C. Di Valentin, C. Wöll, *Sci. Rep.* **2014**, *4*, 3808.

[20] a) D. A. Panayotov, J. T. Yates, *Chem. Phys. Lett.* **2007**, *436*, 204 – 208; b) H. Noei, H. Qiu, Y. Wang, M. Muhler, C. Wöll, *ChemPhysChem* **2010**, *11*, 3604 – 3607; c) E. V. Benvenutti, L. Franken, C. C. Moro, C. U. Davanzo, *Langmuir* **1999**, *15*, 8140 – 8146; d) D. A. Panayotov, S. P. Burrows, J. R. Morris, *J. Phys. Chem. C* **2012**, *116*, 4535 – 4544.

[21] a) D. M. Savory, A. J. McQuillan, *J. Phys. Chem. C* **2014**, *118*, 13680 – 13692; b) T. Berger, J. A. Anta, V. Morales-Flórez, *J. Phys. Chem. C* **2012**, *116*, 11444 – 11455.

[22] C. D. Powell, A. W. Daigh, M. N. Pollock, B. D. Chandler, C. J. Pursell, *J. Phys. Chem. C* **2017**, *121*, 24541 – 24547.

[23] a) D. A. Panayotov, J. T. Yates, *J. Phys. Chem. C* **2007**, *111*, 2959; b) D. Panayotov, E. Ivanova, M. Mihaylov, K. Chakarova, T. Spassov, K. Hadjiivanov, *Phys. Chem. Chem. Phys.* **2015**, *17*, 20563 – 20573.

[24] J. J. M. Vequizo, H. Matsunaga, T. Ishiku, S. Kamimura, T. Ohno, A. Yamakata, *ACS Catal.* **2017**, *7*, 2644 – 2651.

[25] D. M. Savory, D. S. Warren, A. J. McQuillan, *J. Phys. Chem. C* **2011**, *115*, 902 – 907.

[26] A. Mahdavi-Shakib, J. Sempel, L. Babb, A. Oza, M. Hoffman, T. N. Whittaker, B. D. Chandler, R. N. Austin, *ACS Catal.* **2020**, *10*, 10207 – 10215.

[27] a) E. Bus, J. T. Miller, J. A. van Bokhoven, *J. Phys. Chem. B* **2005**, *109*, 14581 – 14587; b) E. Bus, J. A. van Bokhoven, *Phys. Chem. Chem. Phys.* **2007**, *9*, 2894 – 2902; c) M. Boronat, P. Concepcion, A. Corma, *J. Phys. Chem. C* **2009**, *113*, 16772 – 16784; d) P. Serna, P. Concepcion, A. Corma, *J. Catal.* **2009**, *265*, 19 – 25; e) A. Aguilar-Tapia, L. Delannoy, C. Louis, C. W. Han, V. Ortalan, R. Zanella, *J. Catal.* **2016**, *344*, 515 – 523; f) N. Masoud, L. Delannoy, H. Schaink, A. van der Eerden, J. W. de Rijk, T. A. G. Silva, D. Banerjee, J. D. Meeldijk, K. P. de Jong, C. Louis, P. E. de Jongh, *ACS Catal.* **2017**, *7*, 5594 – 5603.

[28] a) C. J. Pursell, B. D. Chandler, M. Manzoli, F. Boccuzzi, *J. Phys. Chem. C* **2012**, *116*, 11117 – 11125; b) C. J. Pursell, H. Hartshorn, T. Ward, B. D. Chandler, F. Boccuzzi, *J. Phys. Chem. C* **2011**, *115*, 23880 – 23892; c) H. Hartshorn, C. J. Pursell, B. D. Chandler, *J. Phys. Chem. C* **2009**, *113*, 10718 – 10725; d) B. D. Chandler, S. Kendell, H. Doan, R. Korkosz, L. C. Grabow, C. J. Pursell, *ACS Catal.* **2012**, *2*, 684 – 694; e) T. Ward, L. Delannoy, R. Hahn, S. Kendell, C. J. Pursell, C. Louis, B. D. Chandler, *ACS Catal.* **2013**, *3*, 2644 – 2653; f) J. Saavedra, C. Powell, B. Panthi, C. J. Pursell, B. D. Chandler, *J. Catal.* **2013**, *307*, 37 – 47.

[29] P. K. Tsjeng, R. B. Anderson, *Can. J. Chem. Eng.* **1976**, *54*, 101 – 106.

[30] M. A. Vannice, S. H. Hyun, B. Kalpakci, W. C. Liauh, *J. Catal.* **1979**, *56*, 358 – 362.

[31] C. T. Campbell, J. R. V. Sellers, *J. Am. Chem. Soc.* **2012**, *134*, 18109 – 18115.

[32] T. Bürgi, R. Wirz, A. Baiker, *J. Phys. Chem. B* **2003**, *107*, 6774 – 6781.

[33] T. Fujitani, I. Nakamura, T. Akita, M. Okumura, M. Haruta, *Angew. Chem. Int. Ed.* **2009**, *48*, 9515 – 9518; *Angew. Chem.* **2009**, *121*, 9679 – 9682.

[34] a) L. J. Antila, F. G. Santomauro, L. Hammarström, D. L. A. Fernandes, J. Sá, *Chem. Commun.* **2015**, *51*, 10914 – 10916; b) S. H. Szczepankiewicz, J. A. Moss, M. R. Hoffmann, *J. Phys. Chem. B* **2002**, *106*, 7654 – 7658; c) S. H. Szczepankiewicz, A. J. Colussi, M. R. Hoffmann, *J. Phys. Chem. B* **2000**, *104*, 9842 – 9850.

[35] K.-D. Jung, A. T. Bell, *J. Catal.* **2000**, *193*, 207 – 223.

[36] a) S. Wendt, J. Matthiesen, R. Schaub, E. K. Vestergaard, E. Lægsgaard, F. Besenbacher, B. Hammer, *Phys. Rev. Lett.* **2006**, *96*, 066107; b) B. Hammer, S. Wendt, F. Besenbacher, *Top. Catal.* **2010**, *53*, 423 – 430.

[37] J. Soria, J. Sanz, I. Sobrados, J. M. Coronado, A. J. Maira, M. D. Hernandez-Alonso, F. Fresno, *J. Phys. Chem. C* **2007**, *111*, 10590 – 10596.

[38] a) C. Sivadinarayana, T. V. Choudhary, L. L. Daemen, J. Eckert, D. W. Goodman, *J. Am. Chem. Soc.* **2004**, *126*, 38 – 39; b) R. Juárez, S. F. Parker, P. Concepción, A. Corma, H. García, *Chem. Sci.* **2010**, *1*, 731 – 738; c) I. P. Silverwood, S. M. Rogers, S. K. Callear, S. F. Parker, C. R. A. Catlow, *Chem. Commun.* **2016**, *52*, 533 – 536.

[39] a) J. Tao, Q. Cuan, X.-Q. Gong, M. Batzill, *J. Phys. Chem. C* **2012**, *116*, 20438 – 20446; b) X.-L. Yin, M. Calatayud, H. Qiu, Y. Wang, A. Birkner, C. Minot, C. Wöll, *ChemPhysChem* **2008**, *9*, 253 – 256.

[40] a) J. S. Bates, B. C. Bukowski, J. Greeley, R. Gounder, *Chem. Sci.* **2020**, *11*, 7102 – 7122; b) A. Vjunov, M. Wang, N. Govind, T. Huthwelker, H. Shi, D. Mei, J. L. Fulton, J. A. Lercher, *Chem. Mater.* **2017**, *29*, 9030 – 9042; c) L. R. Merte, G. Peng, R. Bechstein, F. Rieboldt, C. A. Farberow, L. C. Grabow, W. Kudernatsch, S. Wendt, E. Laegsgaard, M. Mavrikakis, F. Besenbacher, *Science* **2012**, *336*, 889 – 893.

[41] a) Y. Kim, S. Shin, H. Kang, *Angew. Chem. Int. Ed.* **2015**, *54*, 7626 – 7630; *Angew. Chem.* **2015**, *127*, 7736 – 7740; b) F. T. Wagner, T. E. Moylan, *Surf. Sci.* **1988**, *206*, 187 – 202.

[42] U. Roland, T. Braunschweig, F. Roessner, *J. Mol. Catal. A* **1997**, *127*, 61 – 84.

[43] J. Towns, T. Cockerill, M. Dahan, I. Foster, K. Gaither, A. Grimshaw, V. Hazlewood, S. Lathrop, D. Lifka, G. D. Peterson, R. Roskies, J. R. Scott, N. Wilkens-Diehr, *Comput. Sci. Eng.* **2014**, *16*, 62 – 74.

Manuscript received: October 3, 2020
Accepted manuscript online: January 5, 2021
Version of record online: February 26, 2021

